



PCCP

**Early Events in the Mechanism of Single-Source Chemical Vapor Deposition of Zirconium and Hafnium Diboride: A Computational Investigation**

Journal:	<i>Physical Chemistry Chemical Physics</i>
Manuscript ID	CP-ART-11-2023-005385.R1
Article Type:	Paper
Date Submitted by the Author:	27-Nov-2023
Complete List of Authors:	Prokvolit, Sergei; Case Western Reserve University, Department of Chemistry Mao, Erqian; Case Western Reserve University, Chemistry Gray, Thomas; Case Western Reserve University, Department of Chemistry

SCHOLARONE™  
Manuscripts

## ARTICLE

# Early Events in the Mechanism of Single-Source Chemical Vapor Deposition of Zirconium and Hafnium Diboride: A Computational Investigation

Received 00th January 20xx,  
Accepted 00th January 20xx

DOI: 10.1039/x0xx00000x

Sergei Prokvolit,<sup>a</sup> Erqian Mao,<sup>a</sup> Thomas G. Gray\*<sup>a</sup>

Chemical vapor deposition (CVD) of group 4 metal-diboride ceramics from a single source is a versatile technique that finds many applications from hypersonic flight to microelectronics. Though the kinetics of CVD have been studied extensively—allowing significant process improvements—a mechanistic understanding of the process has yet to be attained. Computations suggest two plausible reaction pathways—one higher-energy and the second lower—that correlate well with experimental results reported in the literature, explaining phenomena such as high-temperature deposition resulting in films overstoichiometric in boron. These insights offer a new perspective that may be instrumental in the rational design of new precursors for single-source CVD.

## Introduction

Borides of the group 4 transition metals (TiB<sub>2</sub>, ZrB<sub>2</sub>, HfB<sub>2</sub>) are hard, infusible, inert solids with good thermal and electrical conductivity.<sup>1–4</sup> Their uncommonly high melting points (3,245°C ZrB<sub>2</sub>, 3,380°C HfB<sub>2</sub>) qualify them as ultra-high temperature ceramics (UHTCs),<sup>5</sup> and this property in conjunction with their resistance to oxidation at high temperatures makes them attractive materials for thermal coatings on hypersonic vehicles.<sup>5,6</sup> TiB<sub>2</sub> and ZrB<sub>2</sub> have found applications in protective coatings for cutting tools, for similar reasons.<sup>7,8</sup> Thin films of these ceramics have also drawn interest as copper and gold diffusion barriers for microelectronics.<sup>9–11</sup> Chemical vapor deposition (CVD) has proved to be a powerful technique for generating such films.<sup>12–14</sup>

Two processes dominate the chemical vapor deposition of group 4 transition metal diboride ceramics: independent-precursor systems centered around metal chlorides,<sup>4,8,15–19</sup> and single-source systems involving metal borohydrides.<sup>20–29</sup> The single-source technique has significant advantages over the independent-precursor system. Films may be deposited at temperatures as low as 200–250°C<sup>20–26,29</sup>, whereas the independent-precursor systems require temperatures in excess of 700–900°C.<sup>4,16–19,30</sup> The films deposited from a single source are cleaner, free of halogen impurities.<sup>8</sup> While the kinetics of

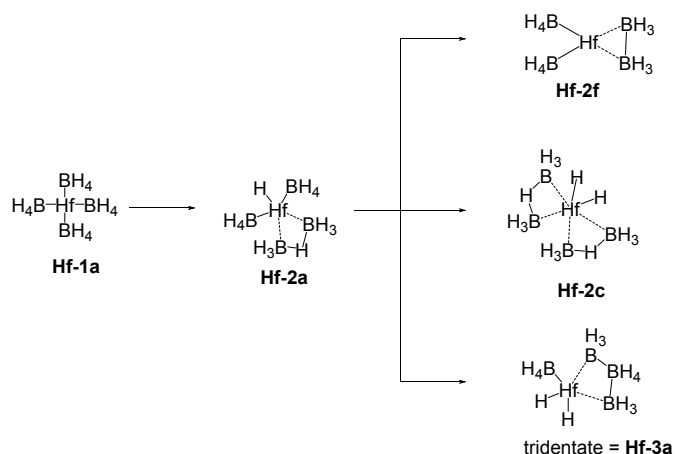
deposition have been studied extensively and this knowledge leveraged to tune the process,<sup>14,22,29</sup> the overall mechanism by which the ceramic is generated has not been elucidated. In this work, we present the results of a computational study of several group 4 metal-borohydride complexes and their reactivities. We discuss the early stages of two probable reaction pathways in the initial stages of deposition. We also contend that these findings have important implications in their own right for the rational design of new CVD precursors.

## Computational Section

Density-functional theory calculations were performed in the gas phase at 298.15 K in Gaussian 16,<sup>31</sup> using the hybrid PBE0<sup>32,33</sup> variant of the PBE<sup>34</sup> functional and Grimme's DFT-D3 dispersion correction with Becke-Johnson damping.<sup>35</sup> This combination has been shown to give satisfactory energetics in main-group and transition element compounds.<sup>36–38</sup> All calculations involving d<sup>0</sup> metal centers were spin-restricted. Both singlet and triplet states were considered for d<sup>2</sup> metal centers; only **Zr-1d** is a ground state triplet. All calculations on open-shell species were spin-unrestricted. Metal centers (Hf, Zr) were described with SDD effective core potentials and basis set,<sup>39</sup> and all other atoms (C, B, H) were defined with the def2tzvp basis set.<sup>40,41</sup> Structures were constructed and visualized in GaussView 06.<sup>42</sup> All starting materials were geometrically optimized, and the potential energy surface subsequently probed with relaxed PES scans. Relevant minima and saddle points turned up by the relaxed PES scans were optimized in turn. Harmonic vibrational frequencies were calculated for all converged structures. Thermodynamic state functions are corrected for zero-point energies and were calculated at 298.15 K from harmonic vibrational frequencies.

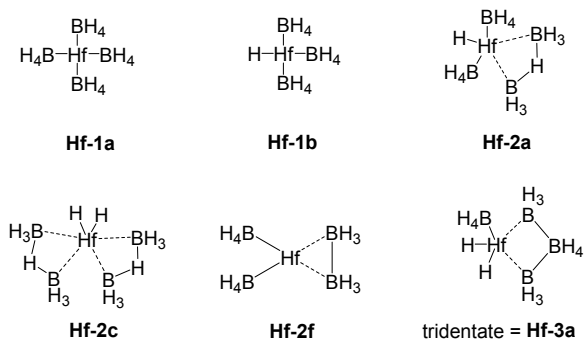
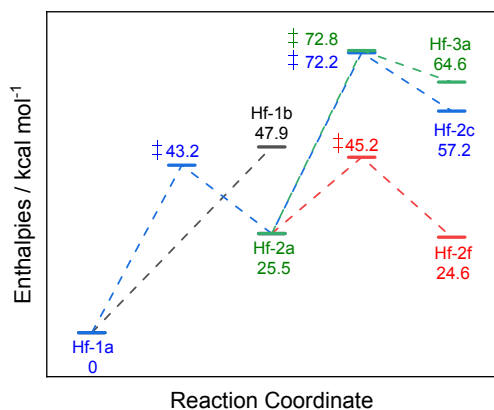
<sup>a</sup> Department of Chemistry, Case Western Reserve University, 10900 Euclid Avenue, Cleveland, Ohio 44106, USA. E-mail: tgray@case.edu

† Electronic Supplementary Information (ESI) available: Discussion and calculations of the spin-orbit coupling contribution to the calculated energies, full reaction maps starting with M(BH<sub>4</sub>)<sub>4</sub> and CpM(BH<sub>4</sub>)<sub>3</sub>, reaction coordinate diagrams for Zr(BH<sub>4</sub>)<sub>4</sub>, CpHf(BH<sub>4</sub>)<sub>3</sub> and CpZr(BH<sub>4</sub>)<sub>3</sub>, visualizations of the structures of **CpHf-2f** and **CpHf-2i**, optimized structures of all complexes investigated in .xyz format, and a .xlsx file containing thermodynamic data and Gaussian input file commands for every structure. This material is available free of charge via the Internet at <http://pubs.acs.org>. See DOI: 10.1039/x0xx00000x

Scheme 1: Initial reactions of  $\text{Hf}(\text{BH}_4)_4$ .

## Results

Four starting materials were investigated:  $\text{Zr}(\text{BH}_4)_4$ ,  $\text{Hf}(\text{BH}_4)_4$ ,  $\text{CpZr}(\text{BH}_4)_3$ , and  $\text{CpHf}(\text{BH}_4)_3$  (where  $\text{Cp} = \text{C}_5\text{H}_5^-$ ). These starting materials are respectively indexed as **Zr-1a**, **Hf-1a**, **CpZr-1a** and **CpHf-1a**. Throughout this work, the indexing system refers to the starting material from which the compound was obtained and the size of the largest boron-based ligand (e.g., **Hf-2a** refers to a complex with a two-vertex borohydride ligand generated from  $\text{Hf}(\text{BH}_4)_4$ ). The final letter provides no further

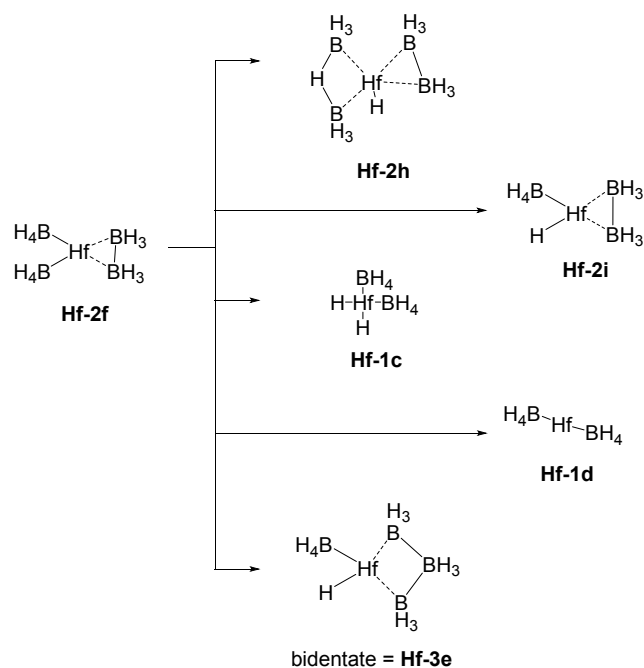
Figure 1: Reaction coordinate diagram of the initial reactions of all  $\text{Hf}(\text{BH}_4)_4$  pathways. All enthalpies were calculated at 298.15 K.

information and was simply assigned according to the order in which geometries were calculated. In some cases, letters have been omitted. This is because a likely geometry was proposed but ultimately not calculated, or was calculated but found to be irrelevant in the context of the overall potential energy surface. Where possible, the same complex with different metal centers has been given the same index designation. When relevant, transition states are indexed such that **Hf-1a-TS-2a** refers to the transition from **Hf-1a** to **Hf-2a**. All enthalpies are given in  $\text{kcal mol}^{-1}$  relative to the respective starting materials. In all optimized structures, stereochemistry at Zr or Hf is approximately tetrahedral, unless otherwise noted.

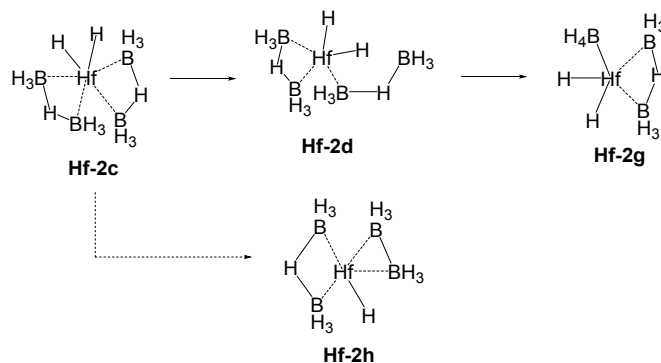
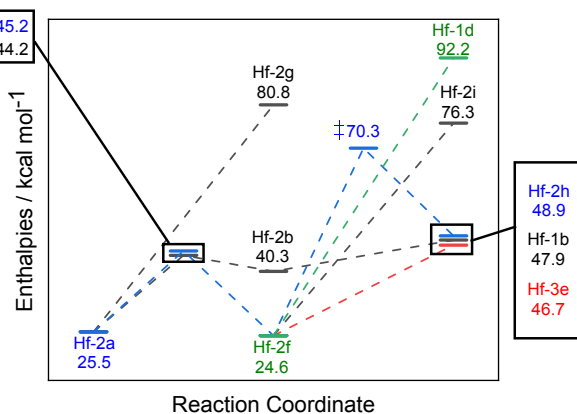
Scheme 1 indicates a trend that recurs for all four precursors: two likely pathways of intramolecular reactions were found, wherein the borohydride ligands reacted with each other while remaining bound to the metal center. One pathway was found to have lower enthalpic demands than nonreactive (i.e. energetically monotonic) dissociation of  $\text{BH}_3$ , while the other pathway was higher in enthalpy. Figure 1 compares these pathways in terms of enthalpy. In both cases the first intermediate was **Hf-2a**, formed through the collision of two  $\text{BH}_4^-$  ligands to produce  $\text{B}_2\text{H}_7^-$  and a terminal metal hydride. The calculated transition state and stable product minimum indicate that this reaction is favored both kinetically and thermodynamically over  $\text{BH}_3$  dissociation.

From **Hf-2a**, the lower energy pathway involved an early elimination of dihydrogen and formation of a diborane dianion, yielding the trigonal planar complex **Hf-2f**. It is important to note that in this reaction the dihydrogen ligand is formed from one terminal metal hydride, and one terminal boron hydride. The higher energy pathway involved further collisions of the borohydride ligands, leading to **Hf-2c** and **Hf-3a**. These reactions are energetically very similar and are likely to compete with each other when they occur. Following the dissociation of  $\text{H}_2$ , **Hf-2f** may convert to several complexes: simple dissociation of  $\text{BH}_3$  to yield the trigonal planar **Hf-2i**, further collisions of the ligands yielding **Hf-3e** (with reduction of the metal center) or square pyramidal **Hf-2h**. Scheme 2 offers a visual summary of these reactions, and Figure 2 compares them beginning from **Hf-2a**, adding for greater context the possible dissociation of  $\text{BH}_3$  from **Hf-2a** either by way of intermediate **Hf-2b**, yielding **Hf-1a**, or directly to yield **Hf-2g**. The transition state **Hf-2a-TS-2b** is energetically close (ca.  $3.7 \text{ kcal mol}^{-1}$ ) to the dissociated product **Hf-1b**. Direct dissociation of  $\text{BH}_3$  or  $\text{B}_2\text{H}_6$  is quite unfavorable, but all the other relevant reactions are thermodynamically similar (though the kinetics vary). Finally, dissociation of the bora-ethane ligand (either as  $\text{B}_2\text{H}_6$  with reduction of the metal center to give the linear **Hf-1d**, or  $\text{B}_2\text{H}_4$  to give **Hf-1c**) is unfavorable, leading to a coordinatively unsaturated metal center.

Note that conversion of **Hf-2f** to **Hf-3e** must obviously go through a transition state, even though none is given. The reaction appears to proceed in two steps. The first is insertion of the metal center into a B-H bond on the complexed dibora-ethane anion, converting the  $\text{B}_2\text{H}_6^{2-}$  ligand into  $\text{B}_2\text{H}_5^-$  and a

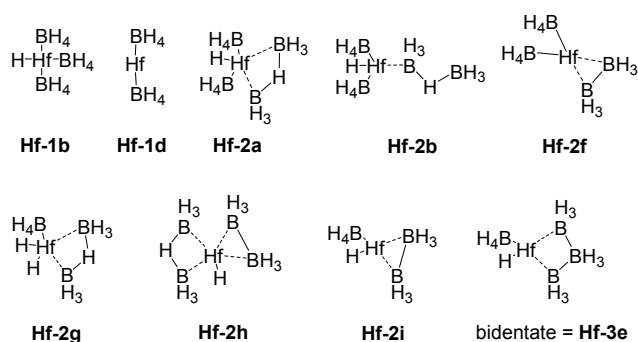
Scheme 2: Reactions along the lower energy pathway of  $\text{Hf}(\text{BH}_4)_4$ .

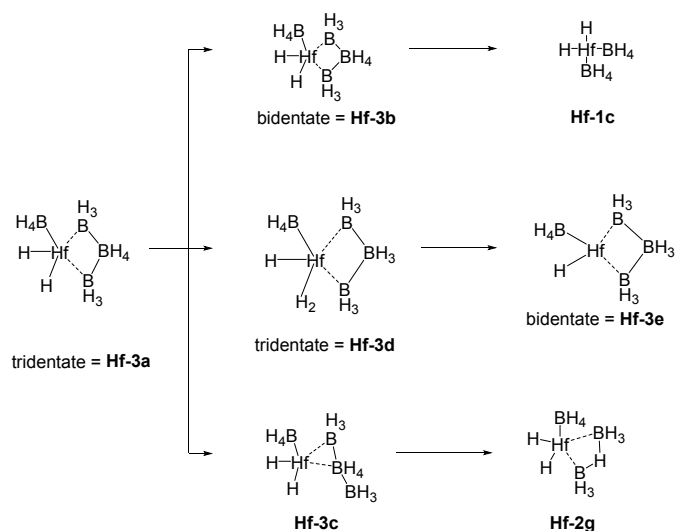
terminal metal hydride. The intermediate converts to **Hf-3e** by a collision of the  $\text{B}_2\text{H}_5^-$  and  $\text{BH}_4^-$  ligands. This mechanism appears to be valid for the  $\text{Zr}(\text{BH}_4)_4$  and  $\text{CpZr}(\text{BH}_4)_4$  complexes as well.

Scheme 3:  $\text{Hf}(\text{BH}_4)_4$  reactions high energy pathway - reactions of **Hf-2c**.

The two higher energy pathways, shown in schemes 3 and 4 and compared in figure 4, are more complex. Conversion of **Hf-2a** into **Hf-2c** and **Hf-3a** is similar kinetically and thermodynamically fairly close; these reactions are likely to compete. Though **Hf-3a** is more expensive in energy, it ultimately leads to the more favorable **Hf-3d** and **Hf-3e** through reductive elimination of  $\text{H}_2$ , much like the low-energy pathway that generates **Hf-2f** (see Figure 2). **Hf-2c**, however, is likely able to convert to **Hf-2h** (see Figure 2, Scheme 3), also a thermodynamically favorable reaction with reductive elimination of dihydrogen (though **Hf-2h** is still slightly less favorable in enthalpic terms). An interesting reaction along this pathway is the reactive elimination of neutral diborane, proceeding through the intermediate **Hf-3b** to yield **Hf-1c**. Dissociation of  $\text{BH}_3$  to give **Hf-2g** remains unfavorable, and in general most of the pathway is higher energy than the dissociation of  $\text{BH}_3$  from **Hf-2a** to give **Hf-1b**.

$\text{Zr}(\text{BH}_4)_4$  gives similar results (see supplemental figures S3-5). Unsurprisingly, the results show that zirconium is more likely to undergo reduction to the +2 state than hafnium. This manifests notably in dissociation of diborane from **Hf-2f** and its zirconium counterpart, **Zr-2f** (see Scheme 2, Figure 2 and supplemental figure S4). Namely, the hafnium complex is much more likely to evolve  $\text{B}_2\text{H}_4$  without reduction of the metal center

Figure 3: Visualization of the structure of **Hf-2f**.

Scheme 4: Hf(BH<sub>4</sub>)<sub>4</sub> reactions high energy pathway - reactions of Hf-3a.

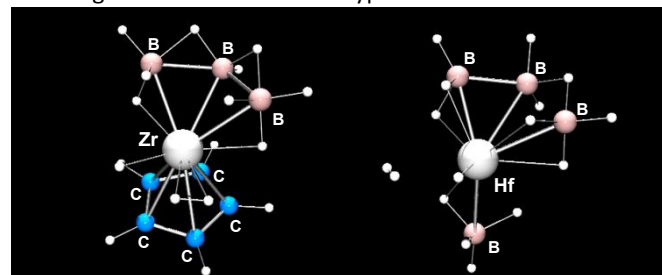
to yield **Hf-1c**. The zirconium complex is somewhat more amenable to dissociation of B<sub>2</sub>H<sub>6</sub> with simultaneous reduction, leaving **Zr-1d**, the only ground-state triplet encountered in this work (see supplemental figure S4). This dissociation remains very unfavorable, leading to an overall enthalpy increase of approximately 18.3 kcal mol<sup>-1</sup> greater than for conversion to **Zr-2i**, and dissociation of B<sub>2</sub>H<sub>4</sub> is higher energy still.

The cyclopentadienyl complexes follow the same overall pattern (see supplemental figures S6-8, S11-13), though the absence of a fourth borohydride ligand in the starting material narrows the possible pathways (e.g. there is no **Hf-2c** equivalent). The Cp<sup>-</sup> ligand appears to encourage reduction and stabilize lower oxidation states of the metal centers by about 7-8 kcal mol<sup>-1</sup>; see Figure 2 and supplemental figures S8, S11 and S16. Most notably, **CpZr-3d** has a neutral B<sub>3</sub>H<sub>9</sub> ligand and a metal center in the +2 oxidation state while its three analogues have a B<sub>3</sub>H<sub>9</sub><sup>2-</sup> ligand and a +4 metal center. Figure 4 shows a visualization of **CpZr-3d** and its analogue, **Hf-3d**. Additionally, an interesting structural difference is the conformation of the B<sub>2</sub>H<sub>6</sub><sup>2-</sup> ligand in complexes **CpZr-2f** and **CpHf-2f** – in lieu of an eclipsed conformation the borane groups are gauche, possibly due to the steric demands of the Cp<sup>-</sup> ligand (see supplemental figures S9-10). Removal of the cyclopentadienyl group in radical form is very high energy, with Δ<sub>r</sub>H = 80-100 kcal mol<sup>-1</sup> for the various complexes investigated.

## Discussion

These computational results correlate well to many experimental observations and offer a new perspective on the mechanism of deposition. Previously, a general scheme of conversion from precursor to product was proposed<sup>43</sup> wherein the reaction proceeded through a metal polyhydride intermediate (indexed in this work as **Hf-1c**; see figure 4, schemes 2 and 4) attained through the loss of diborane (see

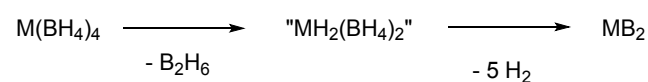
Scheme 5). Several observations supported this conclusion, including volatile diborane as a byproduct of the reaction<sup>20</sup> and

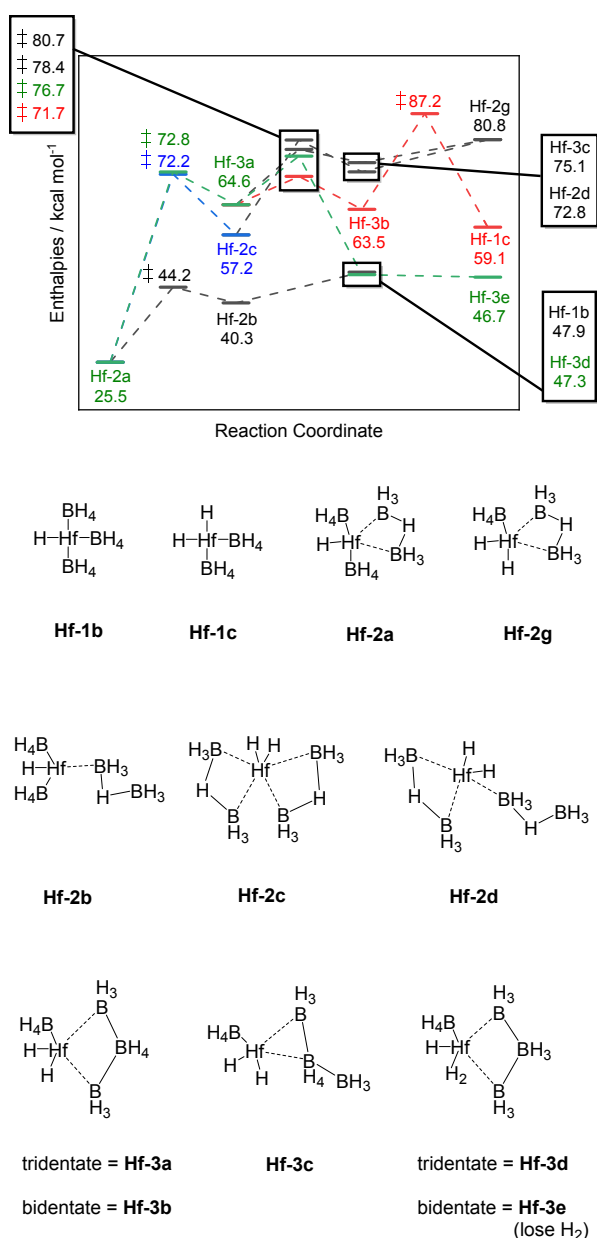
Figure 4: Visualization of the structures **CpZr-3d** and **Hf-3d**. Note the presence of a second bridging hydrogen in **CpZr-3d**. Unlabelled atoms are hydrogen.

the isolation of zirconium and hafnium polyhydrides<sup>43,44</sup> from tetrakis(tetrahydroborato) complexes of the metals in question. It is important to note here the manner in which the polyhydrides were obtained: tetrakis(tetrahydroborato) metal complexes were treated with phosphines, and a neutral phosphine-borane complex was obtained as a byproduct.<sup>43,44</sup> Such a complex would clearly be more stable than the free borane, and therefore less thermodynamically expensive to generate. There is no obviously analogous Lewis base in the deposition mechanism, and therefore it does not necessarily follow that one reaction is representative of the other.

Perhaps based on the scheme proposed by Gozum *et al.*, it appears to have been generally assumed<sup>8,45</sup> that the first step of the deposition mechanism involves the dissociation of neutral borane from the M(BH<sub>4</sub>)<sub>4</sub> complex such that a terminal hydride remains bound to the metal center (with the two BH<sub>3</sub> molecules presumably dimerizing into diborane in the reactor vessel). We observed the possibility of an alternative reaction between two BH<sub>4</sub><sup>-</sup> ligands on the same metal center, to yield a B<sub>2</sub>H<sub>7</sub><sup>-</sup> ligand and a terminal metal hydride. Though still endothermic, we found the products of the intramolecular reaction to be more enthalpically stable by approximately 20 kcal mol<sup>-1</sup>. The transition state for this reaction is comparable to the dissociation products in terms of enthalpies, and generally several kcal mol<sup>-1</sup> lower across the range of compounds studied. By all indications, this reaction is more favorable than the simple dissociation of BH<sub>3</sub>.

The diverging pathways after generation of **Hf-2a** agree roughly with the observation that higher reaction temperatures lead to films overstoichiometric in boron.<sup>8,23-25</sup> The large clusters formed in the higher-energy pathway—more favorable at high temperatures—appear to connect this set of reactions with the generation of polyhedral boron clusters through pyrolysis of diborane: B<sub>3</sub>H<sub>9</sub> has been postulated as an intermediate in the pyrolysis reactions that lead to decaborane(14).<sup>46-48</sup> Furthermore, the presence of a three-vertex boron cage as an intermediate also suggests that these intermediates may convert to the B<sub>3</sub>H<sub>8</sub><sup>-</sup> complexes documented and successfully used as precursors for CVD of metal boride



Scheme 5: Proposed scheme of CVD reaction.<sup>43</sup>Figure 5: Reaction coordinate diagram of the high energy pathway of Hf(BH<sub>4</sub>)<sub>4</sub> reactions. All enthalpies were calculated at 298.15 K.

ceramics.<sup>49</sup> Simple deprotonation of the B<sub>3</sub>H<sub>9</sub> ligand would generate the known B<sub>3</sub>H<sub>8</sub><sup>-</sup>, and the proximity of borohydrides, metal hydrides and cyclopentadienide means that there is high potential for such a reaction to take place. Addition of a reduced metal center to a B-H bond is also a plausible pathway for generation of B<sub>3</sub>H<sub>8</sub><sup>-</sup>. This suggests that the higher-energy pathway does also lead to MB<sub>2</sub> ceramics, albeit the reactions leading to the desired product likely compete with a metal-catalyzed variant of the pyrolysis reactions known to produce higher boranes, leading to excess boron content. Apart from their relevance to the CVD reactions, these findings present an interesting avenue towards metal-assisted synthesis of higher

boranes, a topic of interest in polyhedral boron cluster chemistry.<sup>50–53</sup>

The lower-energy pathway is especially interesting, in part because up to the formation of **Hf-2f** it is both thermodynamically and kinetically favored over any possible avenues of BH<sub>3</sub> dissociation. No clear continuation past **Hf-2f** has presented itself yet – although multiple reactions are possible, all of them are high-energy. It may be that generation of **Hf-2f** is followed by a bimolecular step, e.g. ligands on a second metal-borohydride complex entering the coordination sphere of **Hf-2f**, forming a bridged structure and stabilizing the dissociation of diborane from **Hf-2f**. Though bimolecular reactions were beyond the scope of this particular study, we expect that further investigation of this pathway will lead to energetically favorable bimolecular reactions.

Certain of the B<sub>2</sub> and B<sub>3</sub> ligands here are precedented. The B<sub>2</sub>H<sub>7</sub><sup>-</sup> ligand in **Hf-2a**, **Hf-2b**, **Hf-2d**, **Hf-2c** (twice), **CpHf-2a**, **CpHf-2b**, **CpHf-2c**, and their zirconium analogues, is known. Shore, Bau, *et al.*<sup>54</sup> have reported the crystal structure of [Ph<sub>2</sub>N][B<sub>2</sub>H<sub>7</sub>]. The structure shows a bent geometry at the bridging hydride with staggered BH<sub>3</sub> moieties, giving the anion approximate C<sub>s</sub> symmetry. The measured B–B distance is 2.107(7) Å. Some years later, Green *et al.*<sup>55</sup> disclosed the crystal structure of [CpRu(PMe<sub>3</sub>)(B<sub>2</sub>H<sub>7</sub>)], where the diboron ligand binds analogously to **Hf-2a**. The measured B–B separation is 1.796(6) Å, shorter than that of the free ion. The average B–B separation of B<sub>2</sub>H<sub>7</sub><sup>-</sup> ligands calculated here is 2.061 Å (range: 1.994–2.086 Å) which lies between the experimental values of Shore and Greene. Complex **Hf-2a**, Figure 5(a), is representative: The boron atoms in B<sub>2</sub>H<sub>7</sub><sup>2-</sup> are 2.046 Å apart, and distances between hafnium and the B<sub>2</sub>H<sub>7</sub><sup>-</sup> boron atoms are 2.467 and 2.498 Å. For comparison, the Hf–BH<sub>4</sub> distance is 2.283. The B<sub>2</sub>H<sub>6</sub><sup>2-</sup> ligand of **Hf-2f**, **Hf-2i**, **Zr-2f** and **Zr-2i** is isoelectronic with ethane. This ligand binds early transition elements, as exemplified by Ting and Messerle,<sup>56</sup> Wachter *et al.*<sup>57</sup> and Cotton *et al.*<sup>58</sup>

Only the niobium complex of Wachter and the tantalum complexes of Cotton are crystallographically characterized. In these structures, eclipsed B<sub>2</sub>H<sub>6</sub><sup>2-</sup> ligands bridge metal-metal double bonds between niobium or tantalum. Measured boron-boron bond lengths are 1.716(6) (one niobium complex) and 1.68(2), 1.68(2), and 1.73(2) Å (three crystallographically independent tantalum complexes in two unit cells). The eclipsed geometry presumably maximizes bonding between the dinuclear core and the terminal hydrogens of B<sub>2</sub>H<sub>6</sub><sup>2-</sup>. These bond lengths are shorter than those calculated for the B<sub>2</sub>H<sub>6</sub><sup>2-</sup> complexes here (1.855–1.891 Å). The optimized structure of **Hf-2i** is representative; it appears as Figure 6(b). Moreover, some cyclopentadienyl complexes show *staggered* B<sub>2</sub>H<sub>6</sub><sup>2-</sup> conformations: **CpZr-2f**, **CpHf-2f**; the rest are eclipsed. We are not aware of structurally characterized complexes where B<sub>2</sub>H<sub>6</sub><sup>2-</sup> binds to a single metal atom.

The triboron ligands calculated here appear to be unprecedented among crystallographically authenticated compounds. The [B<sub>3</sub>H<sub>10</sub>]<sup>-</sup> ligands of **Zr-3a**, **Zr-3b**, **Zr-3c**, **Hf-3a**, **Hf-3b**, **Hf-3c**, **CpZr-3a**, **CpZr-3b**, **CpHf-3a**, and **CpHf-3b** are formally hydride adducts of the C<sub>2</sub> isomer of B<sub>3</sub>H<sub>9</sub> calculated by Schaefer,<sup>59</sup> Duke,<sup>60</sup> McKee,<sup>61</sup> and their respective co-workers.

The optimized structure of **Hf-3b** appears as Figure 7(a) and line-drawings of triboron moieties appear as Figure 7(b) and (c).

involving at least one reduction of the metal center, and perhaps multiple cycles of reduction and oxidation as

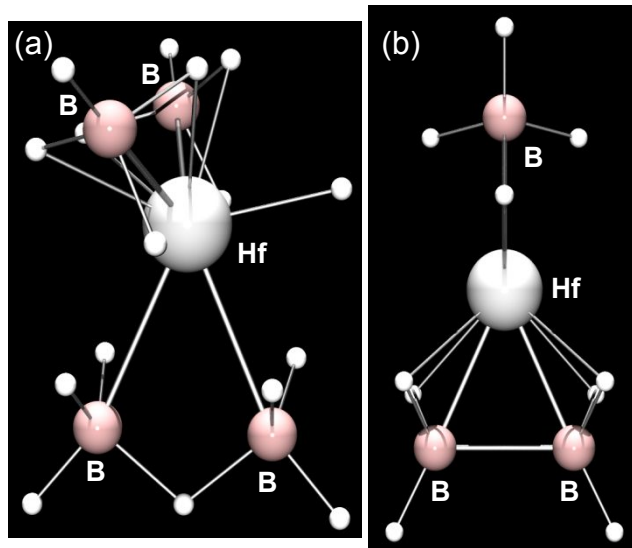


Figure 6: Optimized structures of (a) **Hf-2a**, showing a  $B_2H_7^-$  ligand at bottom, and (b) **Hf-2i**, showing an eclipsed  $B_2H_6^{2-}$  ligand at bottom. Unlabelled atoms are hydrogen.

Whereas  $C_2-B_3H_9$  might be viewed as a di-borohydride adduct of  $BH_2^+$ ,  $C_{2v}-B_3H_{10}$  is a di-(borane) adduct of  $BH_4^-$ .

The neutral ligand  $B_3H_9$  occurring in **CpZr-3d** has few precedents, despite extensive study of triboron intermediates in the pyrolysis of primary boranes.<sup>62–65</sup> The optimized structure of **Hf-3e** appears as Figure 8(a). Perhaps the nearest is a tetraborane(10) isomer calculated at the MP2/6-31G(d,p) level by Ramakrishna and Duke<sup>66</sup> in a study of bis(diboranyl) rearrangement to *arachno*- $B_4H_{10}$ . Line drawings of this isomer and the  $B_3H_9$  ligand calculated here appear as Figure 8(b) and (c). The tetraborane structure may be considered as a  $BH_2^+$  adduct of the  $B_3H_9^{2-}$  ligand encountered here. However, this (unknown)  $B_4H_{10}$  isomer is relatively high in energy, and Ramakrishna and Duke disfavored it as an intermediate in  $B_4H_{10}$  rearrangement. Metal complexes of  $B_3H_9^{2-}$  as in **Hf-3e** do not appear to have been structurally proven.

## Conclusions

Though the mechanistic hypotheses presented here pertain only to the earlier stages of deposition, they offer several useful takeaways for rational design of single-source precursors. Sterically demanding ancillary ligands may help to drive the formation of **Hf-2a** by forcing the  $BH_4^-$  groups closer together. The lower energy barriers observed in the  $CpM(BH_4)_3$  complexes tend to support this hypothesis. The possibility of addition of the metal center into terminal B-H bonds of complexed boranes and borohydrides, followed by reductive elimination of  $H_2$  provides a clear route for dehydrogenation of the borohydride ligands – and, crucially, one that may be tuned. Our calculations find that borohydride ligands are *non-innocent* and that deposition proceeds through formation and degradation of larger boron cages on the metal center –

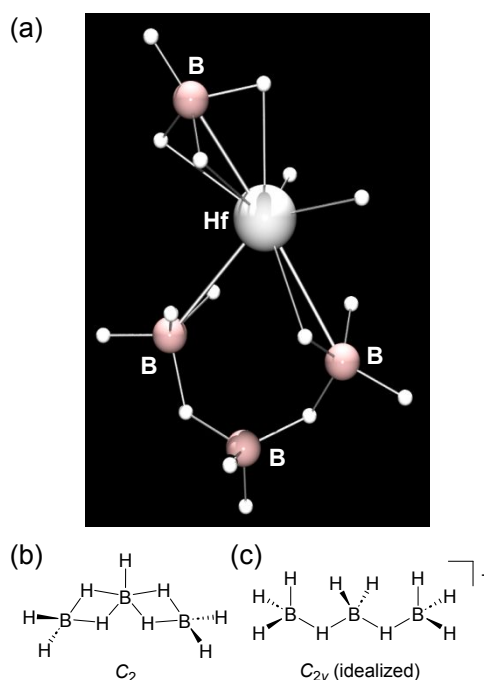


Figure 7: (a) Optimized structure of **Hf-3b**, which is representative of  $B_3H_{10}^-$  complexes. (b) Line drawing of  $C_2$  symmetric  $B_3H_9^-$ . (c) Line drawing of a linear conformation of  $B_3H_{10}^-$ . Unlabelled atoms are hydrogen.

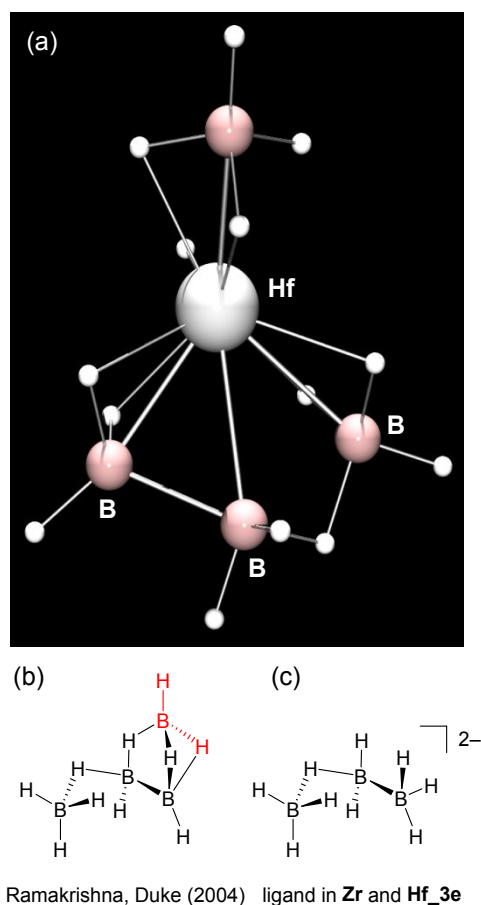


Figure 8: (a) Optimized structure of **Hf-3e**, showing  $B_3H_9^{2-}$  ligand at bottom. (b) Line drawing of a calculated isomer of  $B_3H_{10}$  (see text). (c) Line drawing of calculated  $B_3H_9^{2-}$  ligand. Unlabelled atoms are hydrogen.

dihydrogen ligands are iteratively dispelled. Non-innocence of boron hydride ligands suggests new ideas and research.

We note that the results presented in this work have not been directly corroborated through physical experimentation. Furthermore, common techniques<sup>67</sup> used to investigate deposition reactions are unlikely to shed much light on our findings. For example, mass spectrometry of volatiles may not distinguish between the complexes **Hf-1a**, **Hf-2a**, and **Hf-3a** as they are fully isomeric and may not fragment in a manner that would allow them to be differentiated. IR reflection-absorption spectroscopy shows promise in this regard, and may corroborate these findings in the future.<sup>68</sup> As we continue our investigations, we intend to identify reaction pathways that may be evaluated experimentally.

In summary, early events in the chemical vapor deposition mechanism of zirconium and hafnium diboride ceramics have been discussed. The pathways identified conform to published experimental results, but offer a fundamentally different perspective on the process. Our results suggest that the borohydride ligands react with each other to form larger borohydride and borane intermediates *while bound to the metal center* rather than dissociating as neutral boranes and presumably forming diborane in the gas phase, followed by elimination of dihydrogen. This has implications in the rational design of new CVD precursors, though further investigation is

needed to better understand the proposed pathway and to experimentally corroborate the new hypotheses. Work in this direction is ongoing.

## Author Contributions

Thomas G. Gray: Conceptualization, funding acquisition, investigation, methodology, supervision, and writing – review & editing. Sergei Prokvolit: data curation, formal analysis, investigation, methodology, writing – original draft, and writing – review & editing. Erqian Mao: investigation, methodology, writing – review & editing.

## Conflicts of interest

The authors have no conflicts of interest to declare.

## ORCID ID Numbers

T. G. Gray: 0000-0003-1756-8877

S. Prokvolit: 0009-0009-4900-7338

## Acknowledgements

We thank Prof. Shane Parker for insightful conversations and Dr. Greg Sutton for editorial assistance. S.P. acknowledges a SOURCE fellowship from Case Western Reserve University. This work was funded by the Office of Naval Research, contract N00014-21-1-2230 to T. G. G. This work made use of the High Performance Computing Resource in the Core Facility for Advanced Research Computing at Case Western Reserve University.

## Notes and references

- 1 W. G. Fahrenholtz, G. E. Hilmas, I. G. Talmy and J. A. Zaykoski, *J. Am. Ceram. Soc.*, 2007, **90**, 1347–1364.
- 2 W. G. Fahrenholtz, E. J. Wuchina, W. E. Lee and Y. Zhou, *Ultra-High Temperature Ceramics: Materials for Extreme Environment Applications*, John Wiley & Sons, Inc., Hoboken, NJ, 2014.
- 3 W. G. Fahrenholtz and G. E. Hilmas, *Scr. Mater.*, 2017, **129**, 94–99.
- 4 J. K. Sonber, T. S. R. C. Murthy, S. Majumdar and V. Kain, *Mater. Perform. Charact.*, 2021, **10**, 89–121.
- 5 E. Wuchina, E. Opila, M. Opeka, W. Fahrenholtz and I. Talmy, *Electrochem. Soc. Interface*, 2007, **16**, 30–36.
- 6 N. P. Pature, *Nat. Mater.*, 2016, **15**, 804–809.
- 7 N. Schalk, M. Tkadletz and C. Mitterer, *Surf. Coatings Technol.*, 2022, **429**, 127949.
- 8 B. W. Lamm and D. J. Mitchell, *Coatings*, 2023, **13**, 266–294.
- 9 J. S. Chen and J. L. Wang, *J. Electrochem. Soc.*, 2000, **147**, 1940–1944.
- 10 *US Pat.*, US661408281, 2003.
- 11 J. R. Shappiro, J. J. Finnegan and R. A. Lux, *J. Vac. Sci.*

- 12 *Technol. B Microelectron. Nanom. Struct.*, 1986, **4**, 1409.
- J. Sung, D. M. Goedde, G. S. Girolami and J. R. Abelson, *J. Appl. Phys.*, 2002, **91**, 3904–3911.
- 13 J. Sung, D. M. Goedde, G. S. Girolami and J. R. Abelson, *Mater. Res. Soc. Symp. - Proc.*, 1999, **563**, 39–44.
- 14 J. R. Abelson and G. S. Girolami, *J. Vac. Sci. Technol. A Vacuum, Surfaces, Film.*, 2020, **38**, 30802.
- 15 J. F. Pierson, T. Belmonte and H. Michel, *J. Phys. IV Proc.*, 2001, **11**, Pr3/85.
- 16 R. Naslain, J. Thebault, P. Hagenmuller and C. Bernard, *J. Less-Common Met.*, 1979, **67**, 85–100.
- 17 B. N. Beckloff and W. J. Lackey, *J. Am. Ceram. Soc.*, 1999, **82**, 503–512.
- 18 S. Motojima, K. Funahashi and K. Kurosawa, *Thin Solid Films*, 1990, **189**, 73–79.
- 19 M. Mukaida, T. Goto and T. Hirai, *J. Mater. Sci.*, 1991, **26**, 6613–6617.
- 20 S. Jayaraman, Y. Yang, D. Y. Kim, G. S. Girolami and J. R. Abelson, *J. Vac. Sci. Technol. A Vacuum, Surfaces, Film.*, 2005, **23**, 1619–1625.
- 21 N. Kumar, Y. Yang, W. Noh, G. S. Girolami and J. R. Abelson, *Chem. Mater.*, 2007, **19**, 3802–3807.
- 22 Y. Yang, S. Jayaraman, D. Y. Kim, G. S. Girolami and J. R. Abelson, *Chem. Mater.*, 2006, **18**, 5088–5096.
- 23 J. A. Jensen, J. E. Gozum, D. M. Pollina and G. S. Girolami, *J. Am. Chem. Soc.*, 1988, **110**, 1643–1644.
- 24 G. W. Rice and R. L. Woodin, *J. Am. Ceram. Soc.*, 1988, **71**, C-181-C-183.
- 25 S. Reich, H. Suhr, K. Hanko and L. Szepes, *Adv. Mater.*, 1992, **4**, 650–653.
- 26 A. L. Wayda, L. F. Schneemeyer and R. L. Opila, *Appl. Phys. Lett.*, 1988, **53**, 361–363.
- 27 W. Ye, P. A. Peña Martin, N. Kumar, S. R. Daly, A. A. Rockett, J. R. Abelson, G. S. Girolami and J. W. Lyding, *ACS Nano*, 2010, **4**, 6818–6824.
- 28 A. Chatterjee, S. Jayaraman, J. E. Gerbi, N. Kumar, J. R. Abelson, P. Bellon, A. A. Polycarpou and J. P. Chevalier, *Surf. Coatings Technol.*, 2006, **201**, 4317–4322.
- 29 S. Babar, N. Kumar, P. Zhang, J. R. Abelson, A. C. Dunbar, S. R. Daly and G. S. Girolami, *Chem. Mater.*, 2013, **25**, 662–667.
- 30 H. O. Pierson and A. W. Mullendore, *Thin Solid Films*, 1982, **95**, 99–104.
- 31 M. J. Frisch, G. W. Trucks, H. B. Schlegel, G. E. Scuseria, M. A. Robb, J. R. Cheeseman, G. Scalmani, V. Barone, G. A. Petersson, H. Nakatsuji, X. Li, M. Caricato, A. V. Marenich, J. Bloino, B. G. Janesko, R. Gomperts, B. Mennucci, H. P. Hratchian, J. V. Ortiz, A. F. Izmaylov, J. L. Sonnenberg, D. Williams-Young, F. Ding, F. Lipparini, F. Egidi, J. Goings, B. Peng, A. Petrone, T. Henderson, D. Ranasinghe, V. G. Zakrzewski, J. Gao, N. Rega, G. Zheng, W. Liang, M. Hada, M. Ehara, K. Toyota, R. Fukuda, J. Hasegawa, M. Ishida, T. Nakajima, Y. Honda, O. Kitao, H. Nakai, T. Vreven, K. Throssell, J. Montgomery, J. A., J. E. Peralta, F. Ogliaro, M. J. Bearpark, J. J. Heyd, E. N. Brothers, K. N. Kudin, V. N. Staroverov, T. A. Keith, R. Kobayashi, J. Normand, K. Raghavachari, A. P. Rendell, J. C. Burant, S. S. Iyengar, J. Tomasi, M. Cossi, J. M. Millam, M. Klene, C. Adamo, R. Cammi, J. W. Ochterski, R. L. Martin, K. Morokuma, O. Farkas, J. B. Foresman and D. J. Fox, *Gaussian16, Revision C.01*, Gaussian, Inc., Wallingford CT 2016.
- 32 C. Adamo and V. Barone, *J. Chem. Phys.*, 1999, **110**, 6158–6170.
- 33 M. Ernzerhof and G. E. Scuseria, *J. Chem. Phys.*, 1999, **110**, 5029–5036.
- 34 J. P. Perdew, M. Ernzerhof and K. Burke, *J. Chem. Phys.*, 1996, **105**, 9982–9985.
- 35 S. Grimme, S. Ehrlich and L. Goerigk, *J. Comput. Chem.*, 2011, **32**, 1456–1465.
- 36 J. Yang, L. Z. Tan and A. M. Rappe, *Phys. Rev. B*, 2018, **97**, 85130.
- 37 T. Weymuth, E. P. A. Couzijn, P. Chen and M. Reiher, *J. Chem. Theory Comput.*, 2014, **10**, 3092–3103.
- 38 J. Hermann and A. Tkatchenko, *J. Chem. Theory Comput.*, 2018, **14**, 1361–1369.
- 39 D. Andrae, U. Häußermann, M. Dolg, H. Stoll and H. Preuß, *Theor. Chim. Acta*, 1990, **77**, 123–141.
- 40 F. Weigend and R. Ahlrichs, *Phys. Chem. Chem. Phys.*, 2005, **7**, 3297–3305.
- 41 F. Weigend, *Phys. Chem. Chem. Phys.*, 2006, **8**, 1057–1065.
- 42 R. Dennington, T. A. Keith and J. M. Millam, 2016.
- 43 J. E. Gozum, S. R. Wilson and G. S. Girolami, *J. Am. Chem. Soc.*, 1992, **114**, 9483–9492.
- 44 J. E. Gozum and G. S. Girolami, *J. Am. Chem. Soc.*, 1991, **113**, 3829–3837.
- 45 J. M. Rimsza, S. C. B. Chackerian, T. J. Boyle and B. A. Hernandez-Sanchez, *ACS Omega*, 2021, **6**, 11404–11410.
- 46 R. E. Enrione and R. Schaeffer, *J. Inorg. Nucl. Chem.*, 1961, **18**, 103–107.
- 47 W. N. Lipscomb, *Boron Hydrides*, W. A. Benjamin, Inc., New York, 1st edn., 1963.
- 48 R. T. Paine, G. Sodeck and F. E. Stafford, *Inorg. Chem.*, 1972, **11**, 2593–2600.
- 49 D. M. Goedde and G. S. Girolami, *J. Am. Chem. Soc.*, 2004, **126**, 12230–12231.
- 50 M. G. S. Londesborough, R. Macias, J. D. Kennedy, W. Clegg and J. Bould, *Inorg. Chem.*, 2019, **58**, 13258–13267.
- 51 J. Bould, O. Tok, W. Clegg, M. G. S. Londesborough, M. Litecká and M. Ehn, *Inorganica Chim. Acta*, 2023, **547**, 1–7.
- 52 K. Pathak, C. Nandi and S. Ghosh, *Coord. Chem. Rev.*, 2022, **453**, 214303.
- 53 T. P. Fehlner, *Organometallics*, 2000, **19**, 2643–2651.
- 54 S. G. Shore, S. H. Lawrence, M. I. Watkins and R. Bau, *J. Am. Chem. Soc.*, 1982, **104**, 7669.
- 55 P. D. Grebenik, M. L. H. Green, M. A. Kelland, J. B. Leach, P. Mountford, G. Stringer, N. M. Walker and L. L. Wong, *J. Chem. Soc. Chem. Commun.*, 1988, 799–801.
- 56 C. Ting and L. Messerle, *J. Am. Chem. Soc.*, 1989, **111**, 3449.
- 57 H. Brunner, G. Gehart, W. Meier, J. Wachter, B. Wrackmeyer, B. Nuber and M. L. Ziegler, *J. Organomet. Chem.*, 1992, **436**, 313.
- 58 F. A. Cotton, L. M. Daniels, C. A. Murillo and X. Wang, *J. Am. Chem. Soc.*, 1996, **118**, 4830.
- 59 B. J. Duke, C. Liang and H. F. Schaefer III, *J. Am. Chem. Soc.*,

- 1991, **113**, 2884.
- 60 B. J. Duke, J. W. Gauld and H. F. Schaefer III, *J. Am. Chem. Soc.*, 1995, **117**, 7753.
- 61 B. Sun and M. L. McKee, *Inorg. Chem.*, 2013, **52**, 5962–5969.
- 62 N. N. Greenwood and R. Greatrex, *Pure Appl. Chem.*, 1987, **59**, 857.
- 63 J. F. Stanton, W. N. Lipscomb and R. J. Bartlett, *J. Am. Chem. Soc.*, 1989, **111**, 5165.
- 64 W. N. Lipscomb, J. F. Stanton, W. B. Connick and D. H. Magers, *Pure Appl. Chem.*, 1991, **63**, 335.
- 65 B. Sun and M. L. McKee, *J. Phys. Chem. A*, 2013, **117**, 9076–9082.
- 66 V. Ramakrishna and B. J. Duke, *Inorg. Chem.*, 2004, **43**, 8176–8184.
- 67 J. A. J. Glass, S. S. Kher, Y. Tan and J. T. Spencer, *ACS Symp. Ser.*, 1999, **727**, 130–143.
- 68 Z. V Zhang, G. S. Girolami and J. R. Abelson, *J. Vac. Sci. Technol. A Vacuum, Surfaces, Film.*, 2021, **39**, 63221.